Experiments in X-Ray Physics

Lulu Liu (Partner: Pablo Solis)*
MIT Undergraduate
(Dated: October 22, 2007)

We show X-ray physics to be a rich field of study with significant potential impact through a series of short experiments. We demonstrate X-ray production, absorption, emission, and scattering by exploring phenomena such as bremsstrahlung radiation, electron-positron annihilation, characteristic lines of elements, compton scattering, and X-ray attenuation through matter. We find that the characteristic radiation of an element varies quadratically with its atomic number. In addition, we measure cross sections and formulate a rough model for the calculation of cross sections in the range of 10-80 keV.

1. INTRODUCTION

X-rays are photons with energies from 0.1 to 100 keV and are capable of interacting with matter in a number of ways. They were first discovered by Wilhem Roentgen in 1895. Since X-rays are characteristic of many atomic processes, each interaction is poised to give us deeper insight into basic structure and properties of the atom. Here, we choose to perform several basic X-ray physics experiments to demonstrate the regularity of inner-shell atomic structure, the wavelength-dependent nature of X-ray scattering cross section, to explore nuclear and atomic interactions through spectral analysis, and to measure the characteristic emission lines of elements and determine their relationship to the atomic number, Z.

2. EQUIPMENT AND CALIBRATION

We use a solid-state Germanium detector to count and characterize incoming photons. The ionization chamber is cooled to a temperature of 80K to reduce thermal noise, and reverse-biased to -700 VDC to sweep out any electrons excited into the conduction band. The set up is hooked up through an amplifier to a multi-channel analyser (MCA) which sorts each signal according to its amplitude into anywhere between 1,000 and 10,000 energy bins.

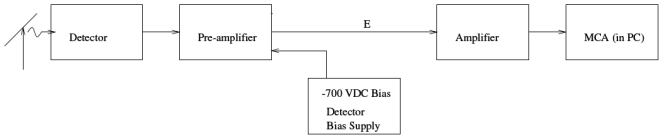

FIG. 1: Schematic of detector set-up. Diagram from 8.13 Lab Guide [3].

We calibrate the MCA (whose response we assume to be linear) with several sources of known energies. In general, two-point calibration is adequate but three points or more are preferred. This particular calibration (most relevant to the investigation of characteristic lines) is done with three known energy sources: Tb $K_{\alpha 1}$ Line (44.5 keV), Mo K_α Peak (17.45 keV), and Fe^{55} radiation (5.89 keV). The plot of their energies vs. recorded bin numbers is shown in Figure 2 and fit by a linear regression.

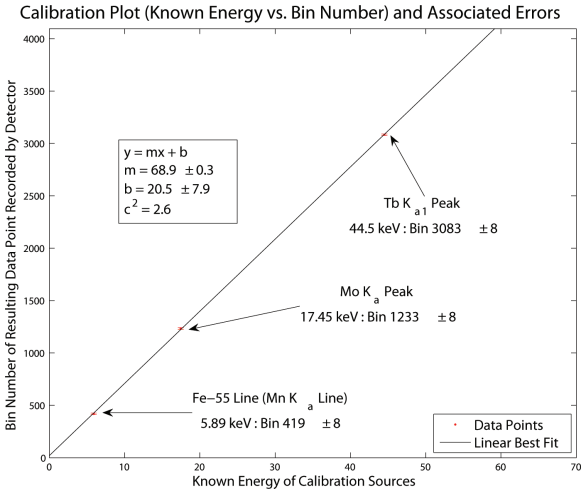

FIG. 2: Three-point linear calibration of the MCA valid in the energy range 0 to 70 keV. Graph of energy vs. recorded channel number for a configuration of 4096 total channels.

The linear relatinoship is used to associate channel numbers with energy values. The subsequent error for this determination is found using error propagation to be,

$$\sigma_E^2 = 0.027 + 4 \times 10^{-9}(N - 20.5)^2 \qquad (1)$$

where E is energy in keV and N is the channel number. The calibration error is a systematic error which also encompasses the random measurement error. This calibration was performed for every energy determination in the following experiment.s

*Electronic address: lululiu@mit.edu

3. PRODUCTION OF HIGH-ENERGY PHOTONS: BREMSSTRAHLUNG RADIATION

3.1. Theory and Set-up

When a charged particle experiences an acceleration, a photon is emitted. Accordingly, an incoming electron passing very close to the nucleus of an atom will be scattered by the electric field of the nucleus and emit radiation, the energy of which is dependent on the magnitude of the deflection it receives. An electron that loses all of its energy in the interaction will emit the minimum allowed wavelength photon- this is considered the short wavelength limit or cut-off energy of the spectrum. It was through observation of this phenomenon that X-rays were first discovered as a form of electromagnetic radiation.

Strontium-90 is the radiation source used in this experiment. The isotope decays in a series of two steps, emitting a beta particle at each stage. Sr^{90} undergoes a series of two beta-decays to become stable Zr^{90}. The maximum kinetic energy electrons, with 2.25 MeV, are emitted by the second of the two processes [1].

$$n \Rightarrow p^{+} + e^{-} + \bar{\nu_e} \tag{2}$$

Taking advantage of the bremsstrahlung phenomenon, we can easily produce a full continuum of X-rays with energies ranging from zero to the maximum kinetic energy of the incident particles using a high Z target (see Figure 3). The implications of this are great. From medical diagnosis to the inner structure of the atom to astronomy and astrophysics, this phenomenon has far reaching impact in many fields of science. We look to demonstrate the production of bremsstrahlung radiation the setup depicted in Figure 3 and deduce from the resulting spectrum the maximum cutoff energy of Sr^{90}.

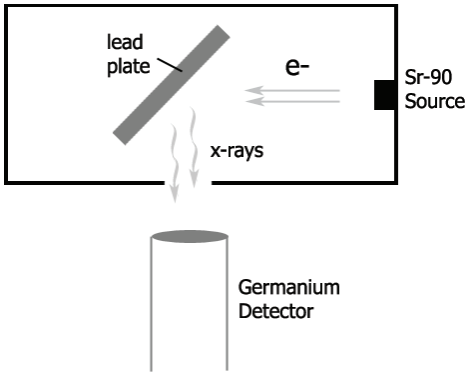

FIG. 3: Apparatus for the production of bremsstrahlung radiation using a Sr^{90} radioactive source.

3.2. Results and Comments

The spectrum obtained from a 20-hour integration period with this setup is shown in Figure 4. The continuum is cut by the K-Lines of lead (visible in the upper left of the plot) and has an upper limit of approximately 2.1 $\pm$ 0.09 MeV, beyond which the readings are dominated by noise, as evidenced by its linearity in log-space. The upper limit is spotted as the junction between two behaviors of the continuous curve, and the error approximated by the calibration mentioned earlier.

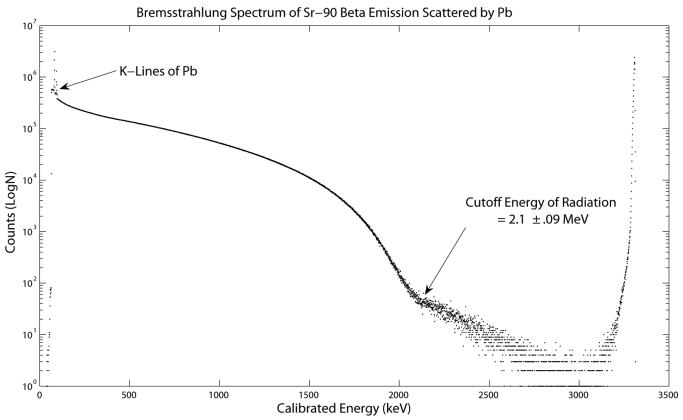

FIG. 4: Bremsstrahlung spectrum of Sr^{90} beta emission onto a lead plate. Key features are labeled.

Since the actual upper limit in kinetic energy for the Sr^{90} decay process is 2.25 MeV, we can see that the beta particle have lost some energy in their trajectories through the source material and through air. In addition, the detector is imperfect in its energy capture and every interaction has a significant probability of producing an escaped photon [1]. Considering the number of interactions necessary for a 2.25 MeV photon to lose all of its energy, the high energy cut-off is likely to be buried by background and thermal noise. However, we see clearly that we were able to generate a continuous wide range of X-rays using a simple set up by taking advantage of the Bremsstrahlung phenomenon.

4. PRODUCTION OF HIGH-ENERGY PHOTONS: ELECTRON-POSITRON ANNIHILATION

In the interest of understanding the sodium-22 decay process, we measure its emission spectrum with our Germanium solid-state detector. In the energy range of 0 to

[1] As evidenced by the identified escape peaks in our investigations to come.

1.5 MeV, the resulting spectrum is shown below in Fig 5.

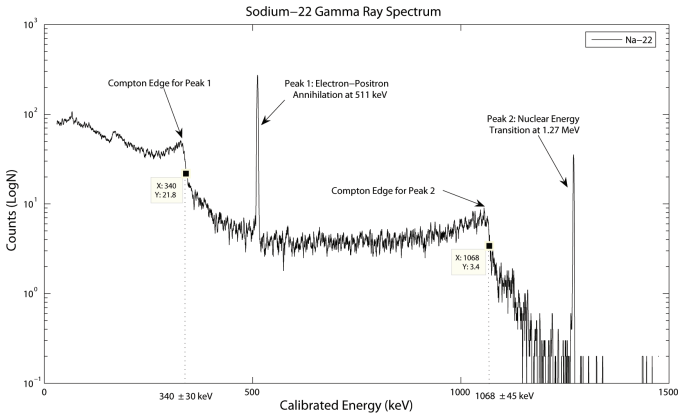

FIG. 5: Spectrum of radiation from a Na^{22} radioactive source. Integration time of 1000s.

We see clearly two sharp peaks in the gamma ray region of the spectrum. One is located at 511 keV and the other at 1.27 MeV. The 511 keV line is the most revealing. It is identical to an electron's rest energy and therefore characteristic of a process in which an electron is completely transformed into a photon with the same energy. This is a clear indication of the occurrence of electron-positron annihilation in Na^{22} atoms, which occurs as a result of nuclear positron decay,

$$p^+ \Rightarrow n + \beta^+ + \nu_e \tag{3}$$

The second, less intense line, is then indicative of a nuclear transition after the β^+ decay. A continuous spectrum of seeming noise with a sharp edge feature follows closely each peak. We hypothesize that due to their continuous nature and their distinguishing cutoff value, these spectra are evidence of Compton scattering (a form of incomplete energy transfer) within the Germanium detector. We confirm this with a calculation.

In Compton scattering, a photon scatters elastically off an electron (through an angle θ), which then recoils with a kinetic energy equal to the energy lost by the photon in this interaction. The relation between the energy of the scattered photon, E', and the angle of scatter, θ is a function of the initial energy, E, and some physical constants.

$$\frac{1}{E'} - \frac{1}{E} = \frac{1}{m_e c^2}(1 - cos\theta) \tag{4}$$

The recoiled photon then escapes, taking with it its remaining energy, and the energy registered by the Germanium detector is the difference between the energy of the original photon and the energy of the scattered photon. Setting $\theta = \pi$, representative of a head-on collision, we find the maximum energy that can be absorbed by an electron in the detector through this process.

For E = 511 keV, our calculations reveal that the first Compton edge should occur at an energy of 511 - 170 = 341 keV. This is in agreement with our data, which places the edge at 340 ± 30 keV. Similarly, the theoretical result for the second Compton edge, 1058 keV, is also within the error bounds of our experiment, 1068 ± 45 keV. We've verified our hypothesis and it is clear that there is much knowledge to be gained by the study of emission lines.

5. X-RAY FLUORESCENCE: CHARACTERISTIC LINES

5.1. Theory and Motivation

When we observe an element under high-energy radiation, a most shocking feature is revealed: distinct, sharp peaks in the X-ray region that, beyond a certain minimum incident energy, are completely independent in energy of this radiation. They are able to uniquely characterize an element and from one element to another of similar Z, varies little except for a shift in energy. We predict that these emission lines are associated with electron transitions very near to the high Z center of an atom and occur as a result of an inner shell vacancy left by an ionized electron. Its predictability and independence of periodicity is striking indication of the extreme regularity of the inner shell electrons.

A theoretical approximation for the behavior of this system can be obtained by making certain assumptions about these energy transitions. For each distinct characteristic line, we predict that the relationship can be obtained roughly using Bohr's formula for energy transitions in a hydrogenic atom with the introduction of a screening factor σ that reduces the effective charge of the nucleus. For a transition from $n = 2 \rightarrow 1$ (K_α radiation), the formula for the energy of the emitted radiation can be restated as such [2],

$$E_\gamma = Rhc(Z-\sigma)^2\left(\frac{1}{1^2} - \frac{1}{2^2}\right) \tag{5}$$

$$= \frac{3}{4}Rhc(Z-\sigma)^2 \tag{6}$$

where $R = 1.1 \times 10^7 m^{-1}$, h is Planck's Constant, and c is the speed of light. Similar models can be calculated for the K_β and L lines with different constants. We will test the strength of these models against empirical data.

5.2. Experimental Design

We subject eight elements with atomic numbers between 25 and 82 to high energy radiation.

Element	Mn	Cu	Rb	Mo	Ag	Ba	Tb	Pb
Z	25	29	37	42	47	56	65	82

TABLE I: Elements used in the characteristic lines experiment.

The source of the radiation is americium-241, which emits approximately 5.5 MeV alpha particles. The detector and MCA are calibrated according to the method outlined earlier.

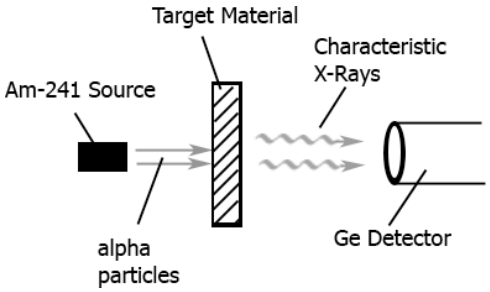

FIG. 6: Experimental schematic for the observation of characteristic lines of elements.

5.3. Data and Plots

Examples of raw data from our experiment is provided here in two forms in Figure 7. $K_{\beta 1}$ and $K_{\beta 2}$ lines result from the K-M ($n = 3 \rightarrow n = 1$) and K-N ($n = 4 \rightarrow n = 1$) transitions, respectively. They appear to be nearly indistinguishable in low Z elements and diverge as Z increases.

The interesting features in Figure 7(b) are indicated with arrows. Note the Ge K_α and K_β escape peaks [2], caused by the loss of one characteristic photon of germanium [3], which has escaped the detector unregistered. The incident photon is recorded with an energy that is lower than its original energy by the K_α energy of Ge, approximately 10 keV.

5.4. Analysis and Fits to Quadratic Curve

We plot $\sqrt{E}$ against atomic number, Z, and find a linear relation (Figure 8), which is consistent with the model described earlier in section 5.1. For the K_α lines, we find the slope of this relation, $\frac{d\sqrt{E}}{dZ}$, to be 0.11 ± 0.01 keV for both $K_{\alpha 1}$ and $K_{\alpha 2}$ lines. This compares favorably with the slope of 0.101 keV predicted by equation 5. The effective screening factor is determined to be 1.6 and 3.0 for $K_{\alpha 1}$ and $K_{\alpha 2}$ lines respectively. For the $K - M(K_{\beta 1})$ and $K - N(K_{\beta 2})$ transitions, the experimentally determined slopes, 0.11 ± 0.01 keV and 0.12 ± 0.01 keV, are also in respective agreement with the predicted slopes of 0.110 and 0.113 keV.

We notice that although two electrons can transition from the same initial energy level to the same final energy level, they can nevertheless emit two slightly different wavelengths of light. The K_α lines, both of which result from a K-L transition, are indistinguishable within our errors at low Z and separate in energy as Z increases. This phenomenon is termed doublet separation and is convincing evidence of a difference in energy in the spin up and spin down states of electrons with the same n and l quantum numbers. Table II is our reduced experimental data on the doublet separation in the p-orbital of the $n = 2$ energy level, as evidenced by our K_α lines.

K-alpha Doublet Separation			
Element	Z	Separation (keV)	Separation Error
Pb	82	2.2	0.30
Tb	65	0.7	0.3
Ba	56	0.2	0.50
Ag	47	0	0.27
Mo	42	0	0.26
Rb	37	0	0.25
Cu	29	0	0.24
Mn	25	0	0.24

TABLE II: Resolution is limited in our determination of doublet separation due to the width of emission peaks as registered by the solid-state detector.

The fourth root of the doublet separation, $(\Delta E)^{1/4}$, when plotted against Z, can be fit by a linear regression of the form $y = a(x - b)$ with a χ^2 of 3.5. Therefore, the difference in energy between the $2p_{1/2}$ and $2p_{3/2}$ electrons follow the general form as predicted by fine structure theory [2],

$$\Delta E = C'(Z - \sigma')^4, \tag{7}$$

6. X-RAY ABSORPTION AND SCATTER: ATTENUATION OF X-RAYS THROUGH MATTER

6.1. Theory and Experimental Motivation

It can be shown that the intensity of a beam of photons passing through matter of constant density and composition decreases exponentially as function of distance traveled,

$$I = I_0 e^{-\rho\sigma x}, \tag{8}$$

where I_0 is the initial intensity of the beam, ρ is the density of the material, and σ is the scattering cross section for the interaction (usually in cm^2/g). Photons scatter in a few main ways off matter: photoelectric absorption (dominant at low energies up to 50 keV), Compton scattering (dominant between 50 keV and 1 MeV), and pair production (5+ Mev)[6]. In the regions we will explore, photoelectric absorption dominates but compton scattering is present. We set up an experiment to determine the behavior of the scattering cross section as we vary the energy and target material.

[2] the K_α escape peak is the largest with higher energy
[3] our ionization solid within the detector

Configuration			K-Beta1 (K-M)				K-Beta2 (K-N)			
Element	Atomic Number	Integration Time	Peak Channel	Peak Energy (keV)	Error on Energy (keV)	Total Count	Peak Channel	Peak Energy	Error on Energy	Total Count
Pb	82	2000	2273	85	5.9	34000	2338	87.5	5.9	19000
Tb	65	679	3462	49.8	0.3	160000	3553	51.1	0.3	42000
Ba	56	907	2548	36.6	0.2	226000	2611	37.5	0.2	32000
Ag	47	1480	1761	25.2	0.2	127000	1761	25.2	0.2	127000
Mo	42	1908	1386	19.8	0.2	68000	1386	19.8	0.2	68000
Rb	37	2000	1058	15.1	0.2	48000	1058	15.1	0.2	48000
Cu	29	1411	631	8.9	0.2	15000	631	8.9	0.2	15000
Mn	25	1100	449	6.3	0.2	36000	449	6.3	0.2	36000

(a)Measured energies of K_β characteristic radiation with associated errors.

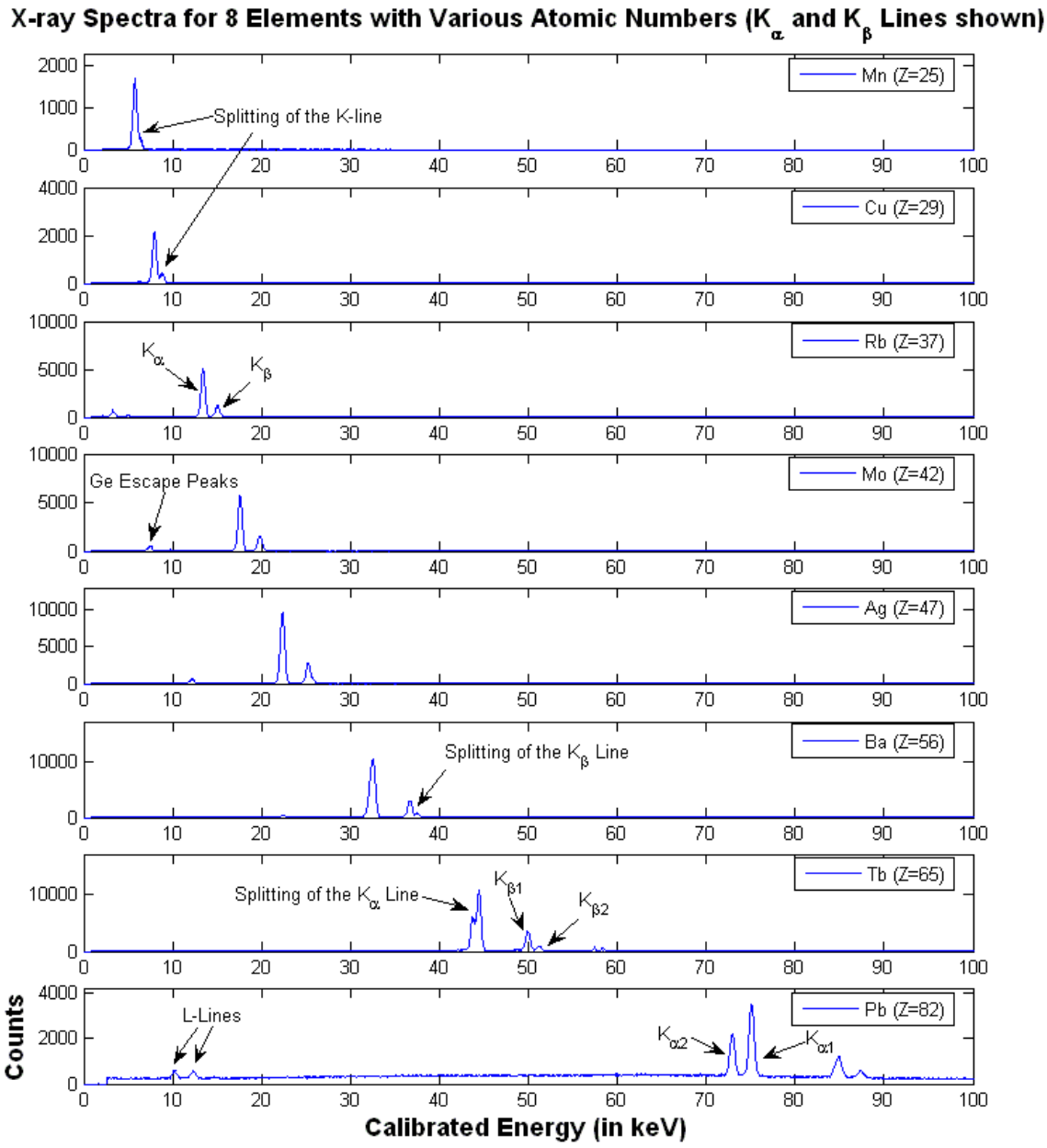

(b)X-ray spectra raw data with removal of high-end noise. The graph has a quadratic quality about it which will become more explicit with analysis.

FIG. 7: Raw spectral data from characteristic lines experiment.

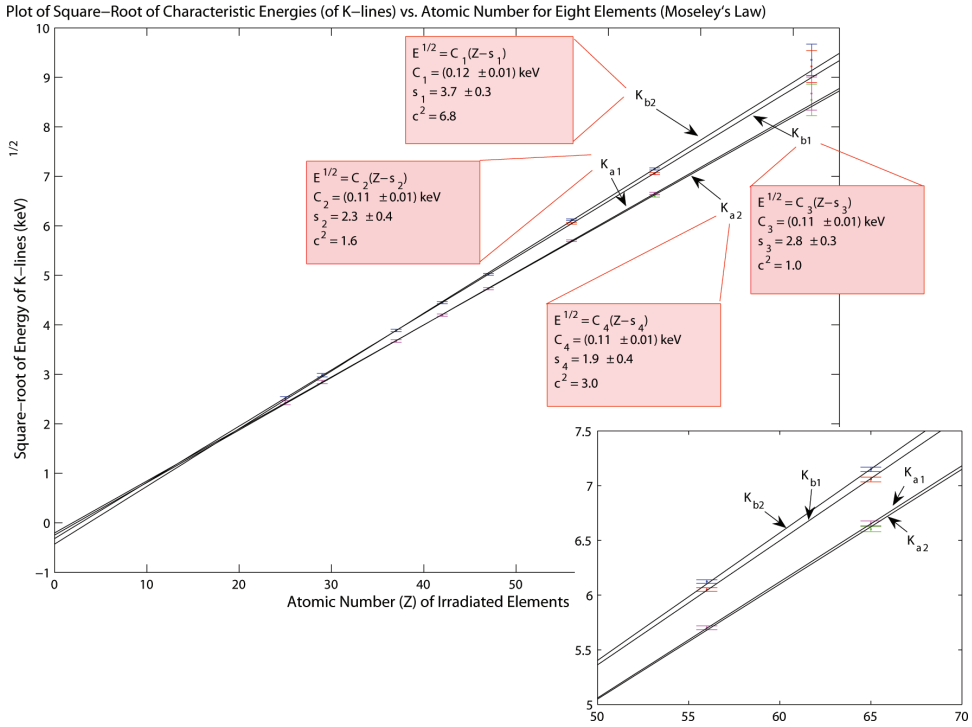

FIG. 8: The relationship between energy of characteristic lines and atomic number of element is quadratic as evidence by this curve, with fit parameters that agree with those expected in a bohr model approximation of the transition.

6.2. Set-up Summary

Our source of monochromatic X-rays are our targets from the characteristic lines experiment described in section 5. Our attenuators are copper, aluminum, molybdenum, and titanium sheets of varying thickness.

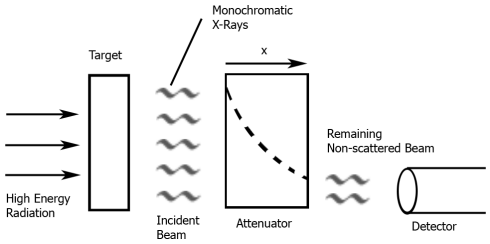

FIG. 9: This diagram shows the set-up for our investigation of X-ray scattering cross sections.

Intensity scales with rate since initial and final energies are the same, the data following is based on rate measurements.

6.3. Data and Analysis

An attenuation curve was obtained for each of seven combinations of energies and attenuators- four energies for a constant attenuator, and four attenuators for a constant energy, with one shared data point. Five trials were

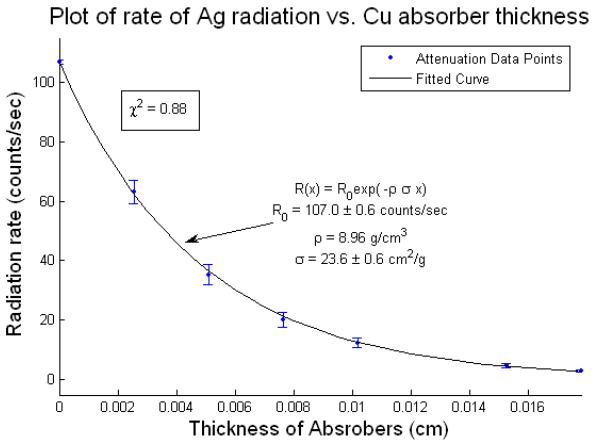

FIG. 10: Plot of rate (in counts/s) vs. attenuator thickness. The attenuator is copper (Z=29) and the radiation is 22.2 keV X-rays emitted by a silver target.

made in the determination of each data point. A linear fit of $Ln(I)$ vs. x was used to find the experimental cross section in each case. The resulting cross sections and errors, along with the χ^2 of their fits, are reproduced below in Table III. We offer the accepted values from NIST for comparison:

The cross section result for the molybdenum attenuator was eventually thrown out because of the lack of data points (only three different thicknesses were obtained) and its too-close proximity to the K-edge of Mo. We de-

Radiation Energy vs. Cross Section Data for Aluminum (Z=13)				
Energy (keV)	Sigma (cm^2/g)	Sigma Error	Actual Sigma	Chi-squared of Fit
13.8	11.5	0.7	10.4	1.2681
22.2	2.7	0.1	2.6	1.1542
50.4	0.36	0.01	0.36	3.0034
75	0.16	0.01	0.21	1.6807

Atomic Number vs. Cross Section Data for E = 22.2 keV				
Z	Sigma (cm^2/g)	Sigma Error	Actual Sigma	Chi-squared of Fit
13	2.7	0.2	2.6	0.52
22	9.8	0.2	11.8	0.93
29	23.6	0.6	25.3	0.88
42	40.2	0.2	71.4	2.72

TABLE III: First table shows the results of experiments with constant Z of attenuator and varying incident photon energies. The second table shows the results of experiments with constant energy and varying Z. Note: though we did our best to avoid absorption edges of the various attenuators, 22.4 keV is very near to the K-edge of Mo.

termined it was not representative of the expected cross section at that energy and atomic number and did not include it in the calculations that follow.

In separate log-log plots of cross section vs. energy and cross section vs. atomic number we find the relations we seek between the three parameters.

$$Ln(\sigma)|_{E=22.2} = m_1 Ln(Z) + b_1 \quad (9)$$
$$m_1 = 2.88 \pm 0.08$$
$$b_1 = -6.6 \pm 0.3$$
$$Ln(\sigma)|_{Z=13} = m_2 Ln(E) + b_2 \quad (10)$$
$$m_2 = -2.5 \pm 0.1$$
$$b_2 = 8.9 \pm 0.2$$

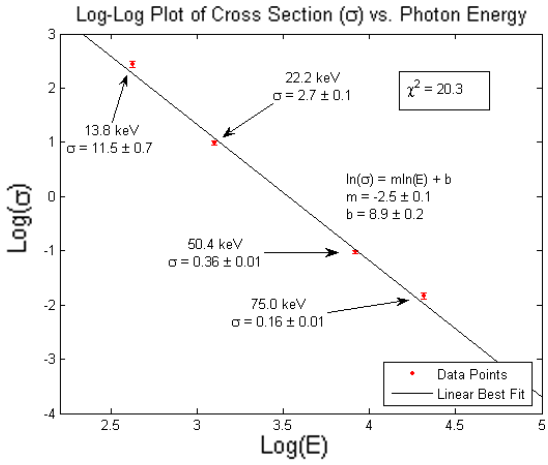

FIG. 11: Cross section σ vs. energy E with Z held constant.

If we imagine the relation to be plotted on a set of three axes, with σ on the z, then by choosing a start point on the surface with either E=22.2 or Z=13 line, we can use the gradient information contained within the set of equations to estimate the value of σ at any other nearby point. We demonstrate the utility of this set of equations and test its predictive powers with experimental data taken for a test data point, 17.4 keV radiation attenuated by Z=29 copper.

The cross section measured for this interaction was $\sigma = 46.5 \pm 0.7 cm^2/g$. Using our set of relations, we obtain a predicted σ of $40.8 \pm 0.6 cm^2/g$. Though they are not in complete agreement, this result is certainly not disappointing and with better experimental data, our model appears promising as a tool to be used in estimating cross sections approximately within the range of our experimental data.

6.4. Statement on Error

The origin of much of the systematic error in this portion of the experiment was uncertainty in the thicknesses of our attenuators. In the case of molybdenum, we believe at least one of the foils was mislabeled, or subject to too much wear and tear, as a thinner foil at one point yielded a lesser average intensity. We chose to throw out these data points because of their obvious invalidity. In the other trials, we chose to factor in thickness uncertainties when calculating uncertainties on rates. In future experiments it will be vital to be certain of our equipment and materials. Random error we tried our best to reduce by performing repeated trials of our measurements and maintaining long integration times. We were able to get this error down to approximately 1%.

At least some error is attributed to the photon beam spreading and an off-90° angle of incidence to the material. More care needs to be taken, however, to align as well as we can the incident beam and the detector hole. Any misalignment, and we're no longer measuring $\theta = 0$, but instead looking at small angle scatter and only some portion of the beam. Moreover, multiple scattering is a concern in thicker foils, and would tend to skew the results toward a smaller cross section, adding positive contribution to the outgoing truly unscattered beam. For more accurate results, especially upon secondary analysis, the experiment should be repeated with careful measurements of all angles and alignments, and subtraction of multiple scattering effects.

7. CONCLUSIONS

We were able to understand a great deal about the inner structures and processes of an atom by analyzing its emission and fluorescence radiation. In our experiment, we demonstrated the extreme regularity of inner shell electron structure in elements with Z greater than 25, and found that characteristic emission results from inner

shell electron energy transitions and can be characterized by a quadratic relating its energy to the atomic number of the element. These characteristic lines uniquely identify an element and do not vary between its elemental and compound form nor alter in chemical reactions. Additionally, we experimentally verified the fine structure theory of doublet separation in spin-up and spin-down electrons for our limited data range.

We produced and characterized Bremsstrahlung radiation using high energy beta radiation and a high Z target. We confirmed the emission of positrons from the nucleus of sodium-22 atoms by recording and analyzing its emission spectrum. We were able to observe compton scattering and edges occuring within the germanium detector, and finally, we were able to find a power-law relationship for the cross section of elemental attenuators as a function of atomic number and energy of incident radiation.

A great wealth of information still stands to be gained through the study of X-ray physics. We have only breached the tip of what is sure to be a very exciting field.

[1] Charles H. Braden et al., 'The Forbidden Beta-Decay of Sr90 and Y90'. Phys. Rev. 75 [Issue 12 June 1949]
[2] Compton and Allison, X-Rays in Theory and Experiment, D. Van Nostrand Company, Inc, [1935]
[3] Sewell, X-Ray Physics, 8.13 Course Reader, [2007]
[4] Melissinos, A.C., Experiments in Modern Physics - 1st Edition, Academic Press, [1966]
[5] Bevington and Robinson, Data Reduction and Error Analysis for the Physical Sciences - 3rd Edition, McGraw-Hill, [2003]
[6] J. H. Hubbell, Pair, Triplet, and Total Atomic Cross Sections, J. Phys. Chem. Ref. [1980].

Acknowledgments

I would like to acknowledge my partner, Pablo Solis, who shared an equal part in this experiment, and the folks at Junior Lab, for all their assistance.